Laser Machining of Ablating/Decomposing Materials — Through Cutting and Drilling Models

Michael F. Modest
Department of Mechanical Engineering
The Pennsylvania State University
University Park, PA 16802

Abstract

A previously-developed three-dimensional conduction model for scribing of a thick solid has been extended to predict the transient temperature distribution inside a finite thickness slab that is irradiated by a moving laser source, and the cutting rate and profile carved by evaporation of material. The laser may operate in CW or in pulsed mode (with arbitrary temporal intensity distribution) and may have an arbitrary spatial intensity profile. The governing equations are solved, for both constant and variable thermophysical properties, using a finite-difference method on a boundary-fitted coordinate system. Results for cutting rates and profiles, as well as for temperature fields, are presented for materials that ablate or decompose upon laser irradiation (without significant formation of liquid), for different material thicknesses, traverse speeds, pulsing conditions, and power levels. For drilling (zero traverse speed), a numerically much more efficient two-dimensional axisymmetric version of the model has also been implemented, and similar results for drilling behavior are presented as well.

Introduction

Since their invention in 1960, lasers have found diverse applications in engineering and industry because of their ability to produce high-power beams. Laser applications include welding, drilling, cutting, scribing, machining, heat treatment, medical surgery, and others. One of the principal advantages of laser cutting is its ability to cut very hard materials easily. Ceramics are among the most difficult materials to machine by conventional machining techniques, since they are very hard and brittle. Lasers may provide a cheaper alternative to conventional machining and have found wide-spread use in industry.

Modeling of laser drilling, cutting and scribing has been addressed by a number of investigators. Simple one-dimensional drilling models have been given by Dabby and Paek [1] and Wagner [2]. Other approximate laser drilling models have been developed by von Allmen [3], Petring *et al.* [4], and others. Multiple reflections during laser drilling have been addressed by Anthony [5], Bailey and Modak [6], Vorreiter *et al.* [7] and Ramanathan and Modest [8].

Simple cutting models have been developed by Bunting and Cornfield [9], and by the group around Schuöcker, e.g., Schuöcker and Müller [10], and Modest and Ramanathan [11].

Laser scribing of ablating and/or decomposing materials has been investigated primarily by Modest and coworkers. They developed a number of simple models for quasi-steady CW laser scribing, e.g., Modest and Abakians [12] and Ramanathan and Modest [13], as well as sophisticated

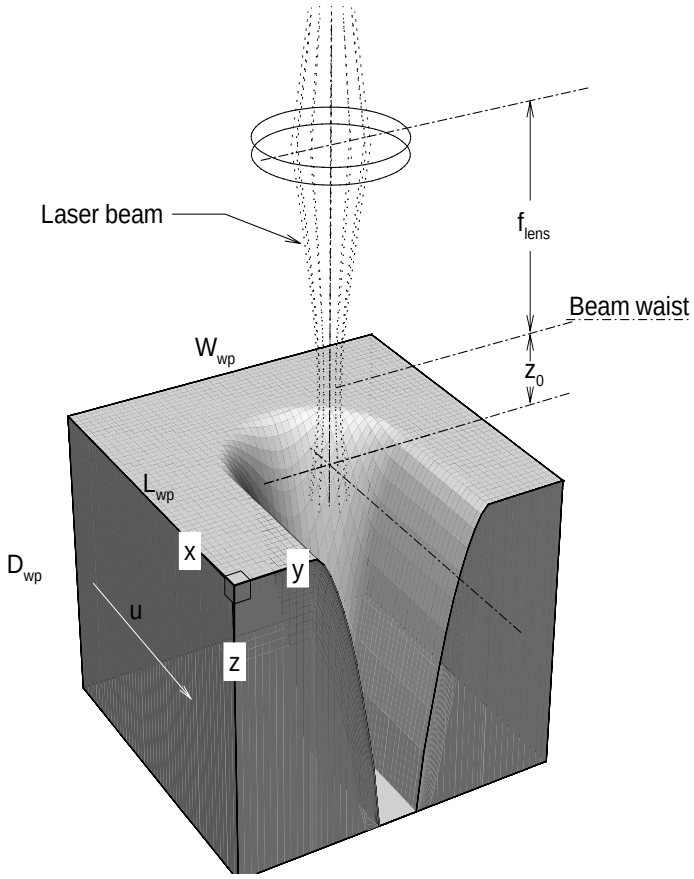

Figure 1: Laser ablation setup and coordinate system.

3-D models for CW as well as pulsed lasers, e.g., Roy and Modest [14], Bang *et al.* [15], Modest [16] and Modest *et al.* [17].

Finally, simple modeling of 3-D machining with a dual beam has been presented by Chryssoloris [18].

In this paper the fully three-dimensional, transient grooving model of Modest [16] is extended to allow accurate modeling of through-cutting. In addition, a two-dimensional axisymmetric version of the model has been developed, in order to predict the results of laser drilling more efficiently.

Theoretical Background

A sketch for the problem under consideration is given in Fig. 1 (for through-cutting). Simplifying assumptions for the present model are more or less identical to the assumptions for the transient, three-dimensional model of Modest [16]; for convenience and to clarify the applicability and limitations of the model, they are repeated here:

1. The solid moves with constant velocity u.
2. The solid is isotropic.

3. Density variations of the solid with temperature are negligible.
4. The material is opaque, i.e., the laser beam does not penetrate appreciably into the medium. This assumption is somewhat limiting since some ceramics and other nonmetals are relatively transparent at shorter wavelengths (i.e., at YAG and excimer laser wavelengths). Even the opaquest material becomes semitransparent during ultra-short pulses compared to thermal penetration by conduction, which may only be a fraction of a μm. Fortunately, for such cases conductive losses are negligible.
5. Change of phase from solid to vapor (or decomposition products) occurs in a single step with a rate governed by a simple Arrhenius relation. This assumption is relatively good for a number of ceramics and other nonmetals, in particular since the exact removal process is not well understood for many materials to date. For example, graphite is expected to ablate, silicon carbide to decompose into various gases, and silicon nitride to decompose into nitrogen and liquid silicon (forming a very thin liquid layer; with droplets being expelled, Ramanathan and Modest [19]). Alumina is known to melt, but the liquid layer may be thin enough due to alumina's low thermal diffusivity. On the other hand the present model is unsuitable for metals, which are expected to form thick liquid layers, possibly with strong convection.
6. The evaporated material does not interfere with the incoming laser beam and ionization of the gas does not occur. Most laser machining devices are outfitted with strong gas assists, which have the purpose of (i) protecting the lens, (ii) blowing debris out of the way, and (iii) suppressing or aiding chemical reactions on the material's surface. Thus, for nonmetals, this assumption is generally good. For metals plasma formation is commonly observed and beam interaction with free electrons is likely in spite of strong gas assist.
7. Multiple reflections of laser radiation within the groove are neglected. In the case of scribing this limits the present analysis to strongly absorbing media and/or shallow grooves. During through-cutting nearly all reflected radiation exits through the bottom opening and is, thus, negligible regardless of the absorptance of the solid. Multiple reflection effects for scribing have been studied by Bang and Modest [20,21] and Bang et al. [15]. Their reflection models could be combined with the present analysis.

As a consequence of these assumptions it is clear that the present analysis is aimed at non-melting ceramics and other nonmetals.

The transient heat transfer equation for a solid (with constant density ρ) of length $L_{wp,}$ width W_{wp} and thickness D_{wp}, with a Cartesian coordinate system fixed to the solid, irradiated by a Gaussian laser beam that moves with constant velocity u into the positive $\overline{x}$-direction (see Fig. 1) may be expressed in terms of temperature T as:

$$\rho c \frac{\partial T}{\partial \overline{t}} = \nabla \cdot (k \nabla T), \tag{1}$$

subject to the boundary conditions,

$$\overline{y} = 0,\ \overline{y} = W_{wp}: \qquad \frac{\partial T}{\partial \overline{y}} = 0, \tag{2}$$

$$\overline{x} = 0,\ \overline{x} = L_{wp}: \qquad \frac{\partial T}{\partial \overline{x}} = 0, \tag{3}$$

$$\overline{z} = \overline{s}(\overline{x},\overline{y},\overline{t}): \qquad \alpha \mathbf{F}\cdot\hat{\mathbf{n}} = -\hat{\mathbf{n}}\cdot(k\nabla T) + h_c(T-T_\infty) + \epsilon\sigma(T^4 - T_\infty^4) + v_n\rho\Delta h_{\text{re}} \tag{4}$$

$$\overline{z} = D_{wp}: \qquad -k\frac{\partial T}{\partial \bar{z}} = h_c(T-T_\infty) + \epsilon\sigma(T^4 - T_\infty^4), \tag{5}$$

and an appropriate initial condition, such as

$$\overline{t} = 0: \quad T(\overline{x},\overline{y},\overline{z},0) = T_\infty, \tag{6}$$

$$\overline{s}(\overline{x},\overline{y},0) = \overline{s}_0(\overline{x},\overline{y}), \tag{7}$$

where v_n is the surface recession velocity (and some quantities have been barred to distinguish the present dimensional quantities from the nondimensional ones introduced below).

Boundary condition (4) states that the irradiation absorbed at the surface is used up by conduction losses into the solid, by convection and radiation losses from the surface, and by evaporation, if present (if no evaporation takes place, *i.e.,* during warm-up, cool-down and in regions too far away sideways from the laser beam, the surface recession velocity vanishes, *i.e.,* $v_n = 0$). The energy intensity distribution, **F**, for a focussed Gaussian laser beam having a waist w_0 at the focal plane z_0, moving with constant velocity u into the positive $\overline{x}$ direction, has been given by Kogelnik and Li [22] and is described in detail in Refs. [14–16]. At the bottom surface, boundary condition (5), conduction out of the solid is balanced by convection and radiation. On both surfaces convection losses are simplified (assuming known, constant heat transfer coefficients h_c), as are radiation losses (assuming gray surfaces surrounded by a vast isothermal enclosure at T_∞). Heat losses from the side walls, equations (2) and (3), are neglected.

In the case of drilling ($u = 0$) the problem becomes two-dimensional if the laser intensity **F** is axisymmetric. The Cartesian coordinate system is then replaced by a cylindrical $\bar{r}, \bar{z}$ system, and boundary conditions (2) and (3) are replaced by

$$\bar{r} = R_{wp}: \quad \frac{\partial T}{\partial \bar{r}} = 0, \tag{8}$$

where R_{wp} is the radius of the solid (disk).

Boundary conditions (2) through (7) are sufficient to solve equation (1) for the temperature if the groove shape $\overline{s}$ is already established ($v_n = 0$) or if v_n is otherwise known. As in Modest [16], we will assume in this paper that the ablation and/or decomposition of the solid material is governed by a simple reaction equation of the Arrhenius type, *i.e.,* the rate of mass loss per unit area is described by

$$\dot{m}'' = \rho v_n = \rho C_1 e^{-E/\overline{R}T}, \tag{9}$$

where E is the decomposition energy, $\overline{R}$ is the universal gas constant, and C_1 is a preexponential factor that depends on the nature of the ablation process (see, *e.g.,* Wei and Ho [23] for simple evaporation).

Before attempting a numerical solution, the governing equations and boundary conditions are non-dimensionalized using the 86%-beam radius at the focal point, w_0:

$$x = \frac{\overline{x}}{w_0}; \quad y = \frac{\overline{y}}{w_0}; \quad \left(\text{or } r = \frac{\bar{r}}{w_0}\right); \quad z = \frac{\bar{r}}{w_0}; \quad s = \frac{\overline{s}}{w_0}; \quad \theta = \frac{T-T_\infty}{T_{\text{re}}-T_\infty}. \tag{10}$$

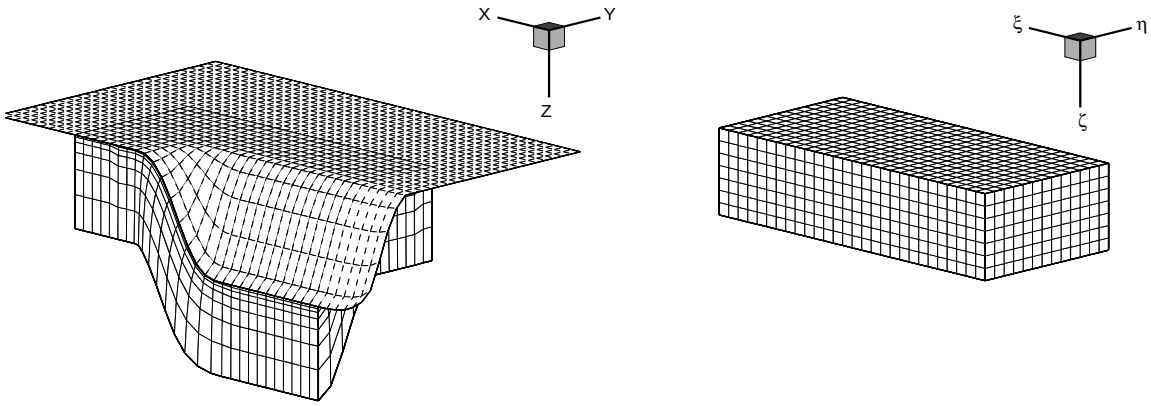

Figure 2: Physical and computational grid systems.

This leads to three basic non-dimensional parameters governing the laser/material interaction:

$$U = \frac{\rho c_{\text{re}} u w_0}{k_{\text{re}}}; \quad N_k = \frac{k_{\text{re}}(T_{\text{re}} - T_\infty)}{F_0 w_0}; \quad \text{Ste} = \frac{\Delta h_{\text{re}}}{c_{\text{re}}(T_{\text{re}} - T_\infty)} \tag{11}$$

(More detail, in particular for variable properties, is given in [16]). Physically, N_k approximates the ratio of conduction losses, for a surface normal to irradiation, and the absorbed laser flux; Ste is a Stefan number that compares ablation energy with sensible heat, and U relates the laser scanning speed to that of thermal diffusion into the medium.

The present set of equations is similar to the ones used previously [16, 17] except that (a) a finite-thickness plate being cut through (rather than grooved) is considered, and (b) convection and reradiation losses from the surfaces are included, primarily to show that such losses are negligible even during cutting of thin plates.

Boundary-fitted coordinates are employed in the numerical solution, *i.e.*, the physical domain (x, y, z) [or (r, z)], is transformed to a uniformly spaced rectangular coordinate region (ξ, η, ζ) (see Refs. [14–16] for details) [or (ξ, ζ) for drilling]. For laser cutting, a two-layered grid system is constructed: a two-dimensional one consisting of $NS_\xi \times NS_\eta$ nodal points to describe the topography of the laser-irradiated surface of the workpiece, and a second, three-dimensional system consisting of $N_\xi \times N_\eta \times N_\zeta$ nodal points to describe that part of the workpiece that is – at any given time – affected by the laser (*i.e.*, whose temperature is raised). This region is bounded by the irradiated surface ($\zeta = 1$), and another surface ($\zeta = N_\zeta$), "far" away into the body not heated by the laser or, if appropriate, by the bottom surface of the workpiece. Grid points of the three-dimensional system at the irradiated surface ($\zeta = 1$) are identical to a subset of the nodal set describing the surface topography. As the laser moves across the surface different parts of the workpiece become heated by the laser beam. Thus, internal nodes are continuously added ahead of the laser beam and dropped in its rear. In Fig. 2 the three-dimensional computational domain (ξ, η, ζ), which is a rectangular parallelepiped, is shown alongside the physical domain which shows the two-tiered nodal system: surface topography nodes are shown by dashed lines, and volume coordinates (corresponding to the parallelepiped of the computational domain) are shown in solid. More details about the two-tiered boundary fitted grids are given in [17]

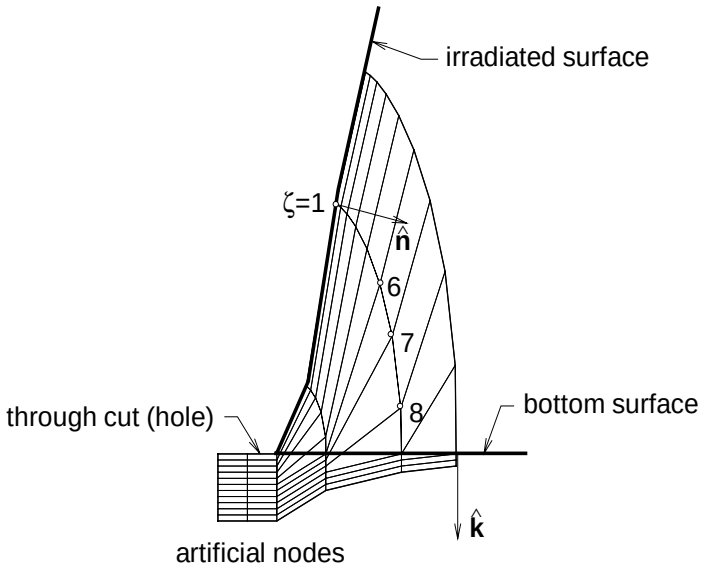

Figure 3: Internal node placement along a (ξ = const, η = const) line near a cut-through location.

Proper placement of internal nodes is important for stability as well as accuracy. Lines of (ξ = const, η = const) need to move smoothly from the top surface (ζ = 1) to a point "far" inside the material (ζ = N_ζ), or all the way to the bottom surface; the various lines may not interfere with one another, indeed, they should stay as far apart as possible everywhere to minimize numerical instability. Near the top surface (where the largest temperature gradients are) the lines need to be perpendicular to the surface (to minimize truncation error [24]). Therefore, the internal nodal system is designed such that the local unit tangent to a (ξ = const, η = const) line is equal to the surface normal near the irradiated surface and blends gradually to the desired gridline direction at a "far-inside" point ζ = N_ζ (see [16] for details). Along the grid lines grid points need to be placed at proper intervals: (a) the grid points should be spaced such that temperature differences from point to point are roughly equal, (b) grid point distance should vary smoothly to minimize truncation error. Thus, many grid points need to be placed near the surface (with its strong temperature gradients), and the spacing needs to gradually open up for larger ζ. It is desirable – for simplicity and compatibility – to maintain an $N_\xi \times N_\eta \times N_\zeta$ brick-shaped nodal system (Fig. 2) even when heat from the laser travels to the bottom surface and/or if through-cutting occurs (*i.e.*, when the 'far-inside' point is below the bottom surface). This is a achieved by adding a thin (hypothetical) layer of material to the bottom of the plate. First, the 'far-inside' point $z > D_{wp}$ is formed, assuming a gridline direction of $\hat{\mathbf{k}}$ (perpendicular to bottom surface) at ζ = N_ζ or the value of ζ at the bottom surface from the previous time step. Let ζ = K be the first node outside the plate. With this knowledge the gridline and its nodal positions are then recalculated such that (i) there are K nodes on the line, (ii) the K-th node lies on the bottom surface,, and (iii) the gridline is perpendicular to the surface at node K. The remaining nodes $K+1, K+2, ..., N_\zeta$ are then staggered a small distance apart directly below node K. A two-dimensional view of a typical internal nodal system near a cut-through location is shown in Fig. 3. For better readability only few nodes are used to cover the heat-affected layer (N_ζ = 12), and the z-spacing of the artificial nodes has been

greatly exaggerated.

The layer is assumed to have the same conductivity as the plate, but zero heat capacity. Therefore, temperature within this layer is quasi-steady as well as one-dimensional (due to its thinness). Assuming constant conductivity in the layer the temperature profile is linear, from equation (1), and given by

$$-k\frac{\partial T}{\partial \overline{z}} = -k\frac{\Delta T}{\Delta \overline{z}} = h_c(T_K - T_\infty) + \epsilon\sigma(T_K^4 - T_\infty^4) \tag{12}$$

The non-dimensionalized and transformed version of equation (1) is finite-differenced and solved using a semi-implicit algorithm. In this scheme θ_ζ and $\theta_{\zeta\zeta}$ (*i.e.*, derivatives normal to the thin heat-affected layer) are finite-differenced implicitly as are the non-linear ablation condition and the reradiation loss terms. All other derivatives are finite-differenced explicitly without loss of stability as explained in [16]. Temperatures in the artifical layer need not be calculated. However, the values of some external nodes are used in some instances to estimate (nearly negligible) cross-derivatives along the bottom surfaces.

Sample Results

The newly developed computer codes were executed for a number of input parameters, to study the effects of sample thicknesses and surface heat losses on laser cutting and drilling of ablating materials, using CW or pulsed lasers. To limit the amount of output data only one set of thermophysical properties and one set of laser parameters were chosen, resulting in "fairly typical" nondimensional parameters of Ste = 2.5 (roughly true for most ceramics, as well as many other nonmetals), N_k = 0.02 and U = 0 (drilling) or 2 (cutting). For example, these conditions could correspond to a P = 200W average absorbed laser power focused to a spot size of w_0 = 150μm, drilling silicon carbide ceramic (U = 0), or cutting it with a scan rate of 5 cm/s (U = 2). In the case of pulsed lasers a non-dimensional pulse duration of τ_p = 0.5 with a 10% duty cycle was chosen. This corresponds roughly (for w_0 = 150μm) to a pulse length of 2.5 ms (400 Hz) with a laser on-time of 250 μs. All calculations were performed on a workpiece large enough that side-wall conditions did not influence the results, and for times large enough that start-up effects also played no role.

Figure 4 shows typical groove cross sections generated by a CW laser cutting specimens of different thicknesses (2.5 and 5 beam radii, and infinitely thick) by scanning into the positive x-direction (measured from the edge of the plate where the laser enters). Four different cross sections are shown: one at the present position of the laser (x = 3.0), and three more in half-beam-radii increments behind the laser. Looking at the case of an infinitely thick plate ($D_{wp} \rightarrow \infty$) one sees that directly under the laser the groove has reached about 2/3 of its final depth (*cf.* the sketch in Fig. 3; only half a beam radius behind the laser the groove has almost reached its maximum depth. More than one beam radius behind the laser all cross sections coincide: no more ablation occurs. Looking at the results for the thin plates, where through-cutting occurs, it is observed that their groove cross sections are almost identical to the ones for an infinite medium (lines are drawn only through the data points for the infinite medium). Only very close to the bottom surface are the grooves a little deeper for thin plates: there is no conduction path further down into the material, freeing a little extra energy for ablation. This was already observed by Ramanathan and Modest [11], who modelled cutting with a simple approximate model.

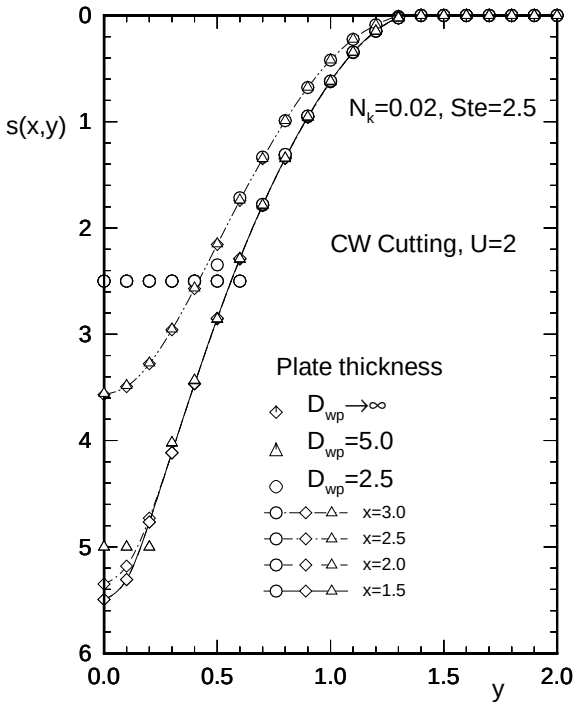

Figure 4: CW laser cutting of plates of varying thicknesses; groove cross sections at various axial locations.

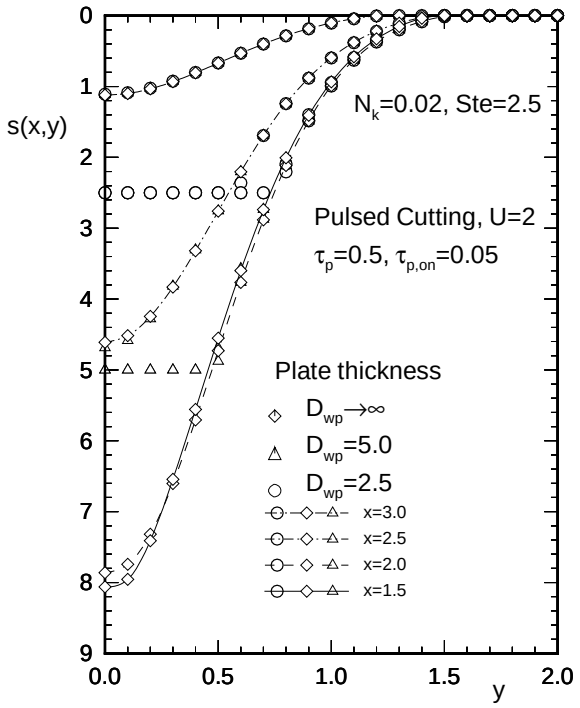

Figure 5: Pulsed laser cutting of plates of varying thicknesses; groove cross sections at various axial locations.

Figure 5 shows the same case as in Fig. 4, but for a pulsed laser. The maximum groove depth is considerably large since conduction losses are much smaller. When the laser reaches x = 3.0 it is about to fire (but has not yet): consequently the groove is rather shallow at that location. Note that there is a difference between the x = 2.0 and 1.5 positions: the laser moves an entire beam radius between any two pulses, resulting in a groove that undulates mildly in depth and width. Looking at the thin plate results it is noticed that the "extra carveout effect" has almost disappeared since conduction losses are very small for a pulsed laser.

Figures 6 and 7 re-examine the influence of the surface losses on the groove shape. It is intuitively difficult to understand that, in the presence of a high-speed gas jet, convection losses are negligible (as compared to ablation energy and conduction losses), as are reradiation losses in spite of the extreme surface temperatures during laser machining (2000K and higher). That these losses are indeed negligible was shown some time ago by Modest and Abakians [12]. Re-examination is in order since Modest and Abakians only examined CW laser machining, did not consider radiation losses (at least not non-linearly), and only made calculations for unrealistically high laser scan rates ($U \geq 10$). In these two figures the maximum possible surface heat losses have been assumed: the maximum heat transfer coefficient for a sonic jet (stagnation point or shear flow) is roughly h_c = 200W/m^{2}K [25], similarly, the maximum reradiation losses occur if the material is black and surrounded by a large enclosure at T_∞. It is seen from Fig. 6 that considering surface losses has a very slight impact on groove shape, and is hardly discernable in the figure. For a pulsed laser the groove shapes are virtually identical (to three significant figures).

The last two figures show some examples from the new two-dimensional drilling model. Figure

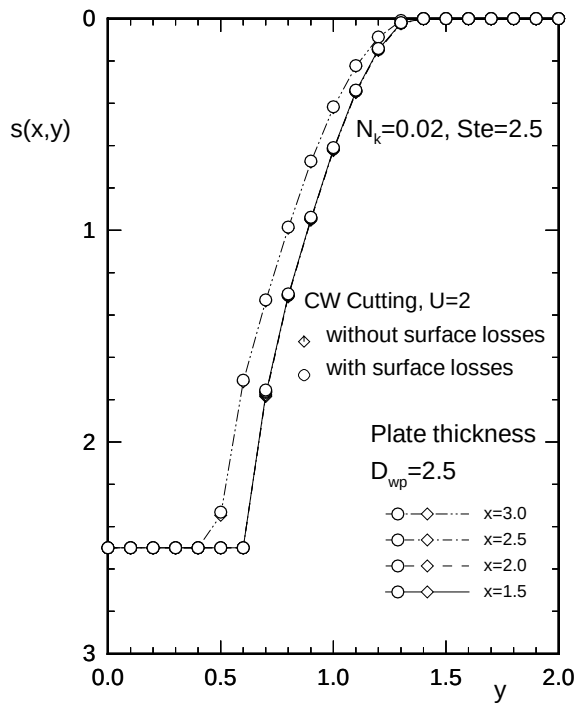

Figure 6: CW laser cutting of thin plates; influence of surface losses by conduction and radiation.

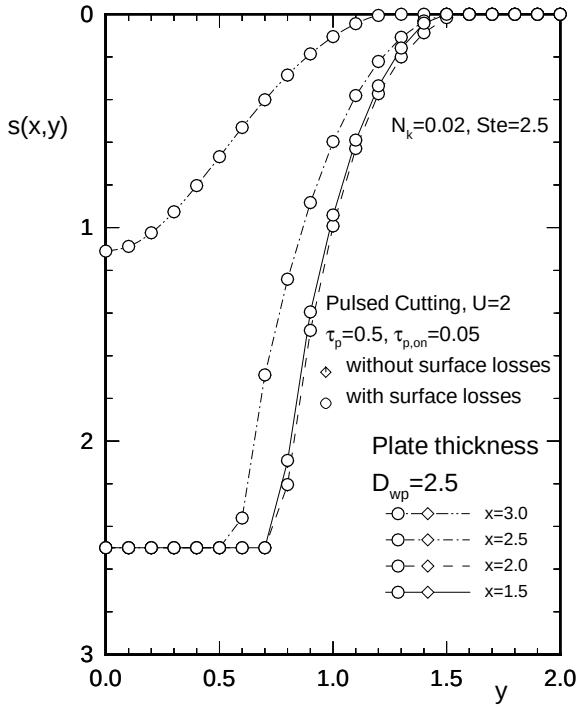

Figure 7: Pulsed laser cutting of thin plates; influence of surface losses by conduction and radiation.

8 shows the hole formation when a specimen, five beam radii thick, is drilled with a CW laser. The calculations have been carried out with, both, the three-dimensional cutting model (symbols) as well as the two-dimensional drilling model (lines). Both models give essentially identical results; the small differences are attributed to the fact that, in the three-dimensional model, a circular geometry is modeled by a square grid, resulting in larger truncation errors.

Finally, Fig. 9 compares the drilling rates of CW and pulsed lasers (both with the same power, etc., as in the previous figures). As was the case for cutting, pulsed lasers achieve considerably larger drilling rates than CW lasers, due to the much lower conduction losses.

Summary and Conclusions

Our three-dimensional conduction model has been extended to allow the prediction of through-cutting of thin specimens, as well as the determination of surface losses by convection and reradiation. It was found that under all circumstances even the maximum possible convection and radiation losses can only have a negligible effect on temperature and groove development.

In addition, to model axisymmetric drilling, a two-dimensional version of the present code was developed. This allows drilling predictions to be made faster by roughly one order of magnitude.

References

1. Dabby, F. W., and U.-C. Paek (1972), High-Intensity Laser-Induced Vaporization and Explosion of Solid Material, **IEEE J. Quantum Electron. QE-8**, 106–111.

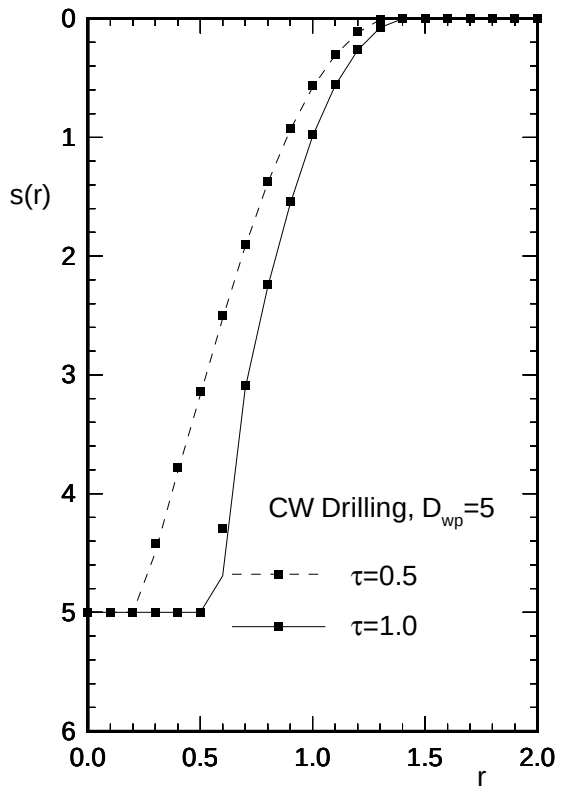

Figure 8: Development of hole cross section during CW laser drilling; comparison of 2D and 3D models.

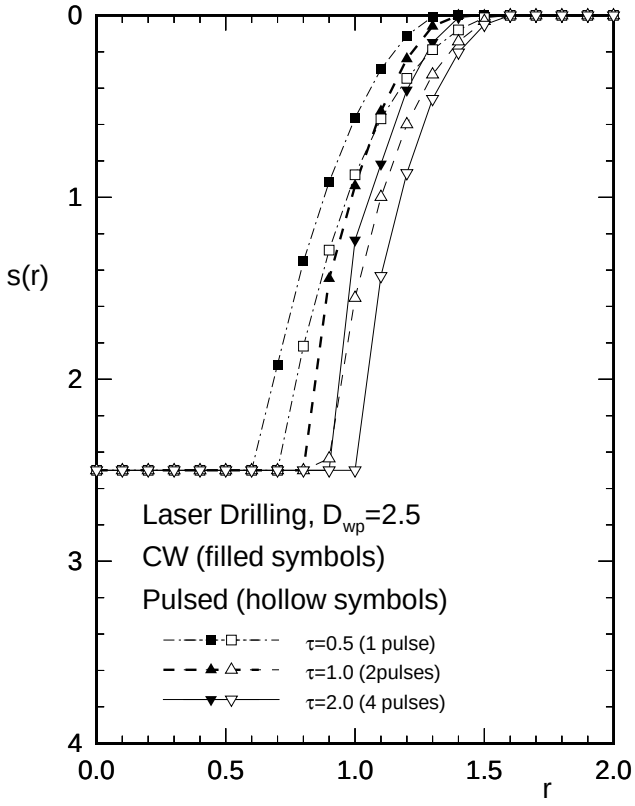

Figure 9: Development of hole cross section during CW and pulsed laser drilling of a thin plate.

2. Wagner, R. E. (1974), Laser Drilling Mechanics, **J. Appl. Phys. 45**, 4631–4637.
3. von Allmen, M. (1976), Laser Drilling Velocity in Metals, **J. Appl. Phys. 47**, 5460–5463.
4. Petring, D., P. Abels, and E. Beyer (1988), Absorption Distribution on Idealized Cutting Front Geometries and Its Significance for Laser Beam Cutting, In *High Power CO_2 Laser Systems and Applications*, 123–131. SPIE, Bellingham, Washington.
5. Anthony, T. R. (1980), The Random Walk of a Drilling Laser Beam, **J. Appl. Phys. 51**, 1170–1175.
6. Bailey, A. W., and A. Modak (1989), Numerical Simulation of Laser Ablation with Cavity Reflections, **J. Thermoph. Heat Transfer 3**(1), 42–45.
7. Vorreiter, J. O., D. A. Kaminski, and R. N. Smith (1991), MonteCarlo Simulation of a Laser Drilling Process, ASME paper no. 91-WA-HT-9.
8. Ramanathan, S., and M. F. Modest (1992), CW Laser Drilling of Composite Ceramics, In *Proceedings of ICALEO '91, Laser Materials Processing*, Vol. 74, 305–326, San Jose, CA.
9. Bunting, K. A., and G. Cornfield (February 1975), Toward a General Theory of Cutting: A Relationship Between the Incident Power Density and the Cut Speed, **J. Heat Transfer**, 116–121.
10. Schuöcker, D., and P. Müller (1987), Dynamic Effects in Laser Cutting and Formation of Periodic Striations, In *Proceedings of the SPIE*, Vol. 801, 258–264.
11. Ramanathan, S., and M. F. Modest (1992), CW Laser Cutting of Composite Ceramics, In *Laser Advanced Materials Processing – LAMP '92*, Vol. 2, 625–632, Nagaoka, Japan.
12. Modest, M. F., and H. Abakians (1986), Evaporative Cutting of a Semi-Infinite Body With a Moving CW Laser, **J. Heat Transfer 108**, 602–607.

13. Ramanathan, S., and M. F. Modest (1990), Effects of Variable Thermal Properties on Evaporative Cutting with a Moving CW Laser, In *Heat Transfer in Space Systems*, Vol. HTD–135, 101–108, ASME.
14. Roy, S., and M. F. Modest (1993), CW Laser Machining of Hard Ceramics — Part I: Effects of Three-Dimensional Conduction and Variable Properties and Various Laser Parameters, **Int. J. Heat Mass Transfer 36**(14), 3515–3528.
15. Bang, S. Y., S. Roy, and M. F. Modest (1993), CW Laser Machining of Hard Ceramics — Part II: Effects of Multiple Reflections, **Int. J. Heat Mass Transfer 36**(14), 3529–3540.
16. Modest, M. F. (1996), Three-Dimensional, Transient Model for Laser Machining of Ablating/Decomposing Materials, **Int. J. Heat Mass Transfer 39**(2), 221–234.
17. Modest, M. F., S. Ramanathan, A. Raiber, and B. Angstenberger (December 1995), Laser Machining of Ablating Materials–Overlapped Grooves and Entrance/Exit Effects, **Journal of Laser Applications 7**(4), 210–218.
18. Chryssolouris, G. (1991), Laser Machining: Theory and Practice, Springer Verlag, New York, NY.
19. Ramanathan, S., and M. F. Modest (1995), High-Speed Photographic Visualization of Laser Processing Phenomena, **Journal of Laser Applications 7**(2), 75–82.
20. Bang, S. Y., and M. F. Modest (1991), Multiple Reflection Effects on Evaporative Cutting with a Moving CW Laser, **J. Heat Transfer 113**(3), 663–669.
21. Bang, S. Y., and M. F. Modest (1992), Evaporative Scribing with a Moving CW Laser—Effects of Multiple Reflections and Beam Polarization, In *Proceedings of ICALEO '91, Laser Materials Processing*, Vol. 74, 288–304, San Jose, CA.
22. Kogelnik, H., and T. Li (1956), Laser Beams and Resonators, **Appl. Opt. 5**(10), 1550–1565.
23. Wei, P. S., and J. Y. Ho (1990), Energy Considerations in High-Energy Beam Drilling, **Int. J. Heat Mass Transfer 33**(10), 2207–2218.
24. Thompson, J. F., Z. U. A. Warsi, and C. W. Mastin (1985), Numerical Grid Generation, Foundations and Applications, North-Holland, New York.
25. Incropera, F. P., and D. P. DeWitt (1990), Fundamentals of heat and Mass Transfer (third Edn), John Wiley & Sons, New York.

Meet the Author

Michael F. Modest was born in Germany and received his Dipl.-Ing. degree in Mechanical Engineering from the Technical University in Munich in 1968. After emigrating to the U.S. he obtained his M.S. and Ph.D. degrees, also in Mechanical Engineering, from the University of California at Berkeley in 1972. He is presently a professor in the Mechanical Engineering Department at the Pennsylvania State University. His research interests cover two major areas in experiment as well as in theory: radiative heat transfer, and heat transfer during laser machining of ceramics.